Using Self-Synchronization Error Dynamics Formulation Based Controller for Maximum Photovoltaic Power Tracking in Micro-Grid Systems

Chao-Lin Kuo, Chia-Hung Lin, Her-Terng Yau, and Jian-Liung Chen

***Abstract*—This paper proposes a self-synchronization error dynamics formulation based controller for maximum photovoltaic power tracking (MPPT) of a photovoltaic (PV) array. The output power conversion of a PV array depends on atmospheric conditions, such as the solar radiation and ambient temperature, and its conversion efficiency is low. Therefore, a MPPT controller is necessary for a PV conversion system, in order to improve the output power. A PV cell is a p-n semiconductor junction. Photon motion, temperature, or electricity conduction cause anomalous diffusion phenomena in inhomogeneous media. In order to describe nonlinear-characteristics, fractional-order calculus can be used to express the dynamic behaviors using fractional-order incremental conductance and to adjust the terminal voltage to the maximum power point. Inspired by the synchronization of Sprott system, a voltage detector is formulated to trace the desired voltage and to control the duty cycle of a boost converter. For a small photovoltaic system, the numerical experiments demonstrate that the proposed method can reduce the tracking time and can improve the conversion efficiency.**

***Index Terms*—Fractional-order calculus (FOC), fractional-order incremental conductance (FOIC), maximum photovoltaic power tracking, photovoltaic (PV) array, self-synchronization.**

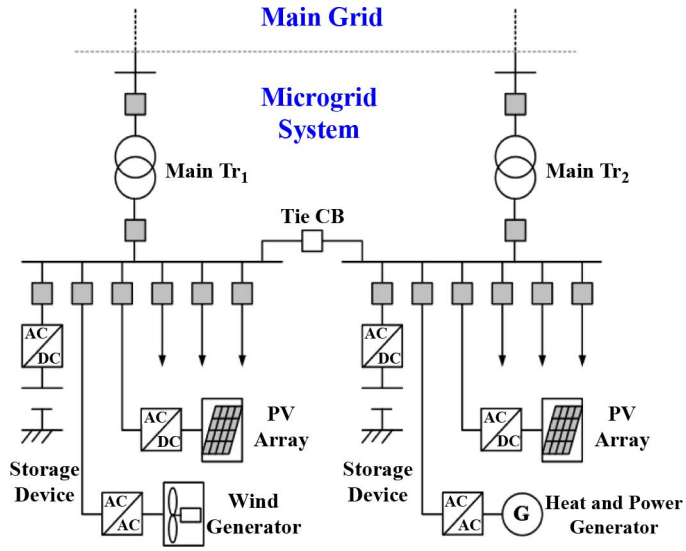

Fig. 1. Structure of microgrid system.

I. Introduction

MICRO-GRIDS are energy management systems that combine local distribution systems and small-scale or medium-scale green energy sources, such as micro-turbines, photovoltaic (PV) systems, wind power systems, distributed storage units, and fuel cells [1]–[3], as shown in Fig. 1. PV conversion systems are widely used, because they directly convert solar radiation energy into electrical power, and their conversion and control systems are simple in their structure and easy to maintain. The applications of PV systems can be divided into standalone systems, grid-connected systems, and battery charge for low-power systems, such as solar heating system, home power supply, and biological science parks [4]–[7]. In micro-distribution systems, grid-connected systems store the solar energy into battery banks, using the dc/dc converters or divert it into local loads using dc/ac inverters, for a single-phase or a three-phase grid-connected model [5]–[9]. However, the output power of a PV system is easily influenced by environmental conditions, such as solar radiation and temperature. Since the solar cell exhibits nonlinear voltage-current and voltage-power characteristics, a maximum photovoltaic power tracking (MPPT) controller must track the maximum power and match the current environmental changes. Many algorithms have been proposed to track the maximum power point, such as the voltage feedback method (VFM), the power feedback method (PFM), current variation reduction control, the perturb and observe method (POM), and the incremental conductance method (ICM) [5]–[13]. These methods use voltage or current adjustment to match the maximum power under varying atmospheric and load conditions.

Artificial intelligence (AI) methods, such as controllers that use neural networks and Fuzzy systems, [14]–[16] can also achieve MPPT. However, AI-based algorithms require a long design cycle to implement in an embedded system, or a microcontroller for home-use, or a small-scale PV conversion system. In addition, many phenomena, such as heat conduction in solids, diffusion viscous flow, flow through

Manuscript received January 19, 2013; revised February 27, 2013; accepted June 27, 2013. Date of publication July 18, 2013; date of current version September 09, 2013. This paper was recommended by Guest Editor G. Chen.

H.-T. Yau is with the Department of Electrical Engineering, National Chin-Yi University of Technology, Taichung City 41101, Taiwan (e-mail: htyau@ncut.edu.tw).

C.-L Kuo is with the Department of Maritime Information and Technology, National Kaohsiung Marine University, Kaohsiung City 81157, Taiwan (e-mail: clkuo@mail.nkmu.edu.tw).

C.-H. Lin and J.-L Chen are with the Department of Electrical Engineering, Kao-Yuan University, Kaohsiung City 821 , Taiwan (e-mail: t21025@cc.kyu.edu.tw).

Color versions of one or more of the figures in this paper are available online at http://ieeexplore.ieee.org.

Digital Object Identifier 10.1109/JETCAS.2013.2272839

porous media, electricity in resistive-capacitative lines, electromagnetic waves, and mass diffusion, demonstrate nonlinear dynamic behavior [17], [18]. Each PV cell is a semi-conducting material (single-crystal, poly crystal, amorphous silicon, and thin film) with a p-n junction (energy band), so photoelectric current, light, and ambient temperature interaction constitute anomalous diffusion. These phenomena can be described as a dynamic behavior such as fractional-order diffusion [19], [20]. Therefore, Grünwald–Letnikov (GL) fractional approximation is proposed to describe the fractional-order incremental conductance (FOIC) for current and voltage changes. Then, inspired by the synchronization of Sprott system [21]–[23], a fractional-order voltage detector is formulated to trace the desired maximum power point voltage and to control the duty cycle of a dc/dc converter. This study uses the FOIC to adjust the duty cycles and the voltages to track the maximum power with time varying. By controlling the duty cycle, the proposed controller can match the load to the PV array under various atmospheric conditions. By applying the proposed approach to a small-scale PV conversion system, the tests show the computational efficiency and a reduction in tracking time.

The organization of this paper is as follows. Section II addresses the problem formulation and motivation, and Section III describes the self-synchronization error dynamics formulation (SEDF)-based voltage detector, including the Sprott system and the fractional-order SEDF. In Sections IV–VI, the implementation of the MPPT controller, the experimental results, and conclusions are given to show the efficiency of the proposed controller.

II. Problem Formulation and Motivation

A PV module is interconnected in a parallel-series configuration to form a PV array that converts solar radiation energy into electrical energy that supplies local loads, and stores the surplus energy in rechargeable batteries in stand-alone and micro-distribution systems [4]–[7]. Each PV cell is a p-n semiconductor junction and its operational characteristics depend on the solar radiation and the surface temperature. It has nonlinear characteristics and its mathematical model can be expressed as [4], [24]

$$I = n_p I_{ph} - n_p I_{\text{sat}} \left[\exp\left(\frac{Q}{bTA} \frac{V}{n_s} \right) - 1 \right] \tag{1}$$

where I is the output current of the PV array, V is the output voltage of the PV array, I_{ph} is the photo-current, I_{sat} is the reverse saturation current, n_p is the number of modules connected in parallel, n_s is the number of modules connected in series, Q is the charge of an electron, b is Boltzmann's constant, A is the p-n junction ideality factor, $1 < A < 5$ ($A = 1$ being the ideal value), and T is the surface temperature of the cell. Currents I_{ph} and I_{sat} both depend on the solar radiation and the cell temperature as [24]

$$I_{\text{sat}} = I_r \left[\frac{T}{T_r} \right]^3 \exp\left(\frac{QE_G}{kA} \left[\frac{1}{T_r} - \frac{1}{T} \right] \right) \tag{2}$$

$$I_{ph} = [I_{sc} + k_{sc}(T - T_r)] \frac{S}{100} \tag{3}$$

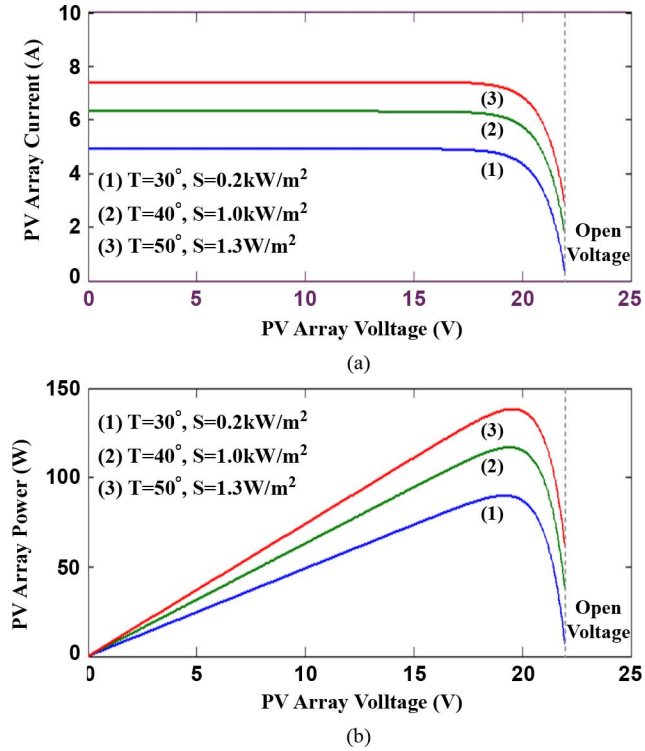

Fig. 2. (a) Characteristic curves of output current versus output voltage (*I-V*). (b) Characteristic curves of output power versus output voltage (*P-V*).

where T_r is the cell reference temperature, I_r is the reverse saturation current at T_r, E_G is the band-gap energy, I_{sc} is the cell short-circuit current at T_r, k_{sc} is the short-circuit current temperature coefficient, and S is the solar radiation in mW/cm^2.

The power of the PV array is computed using $P = I \times V$. The power-voltage (*P-V*) and the current-voltage (*I-V*) characteristic curves of the PV array are nonlinear, as shown in Fig. 2(a) and (b). The average intensity of solar radiation in outer space is approximately $1.366\text{kW}/\text{m}^2$. However, the output characteristics of PV cells are heavily influenced by the atmospheric conditions, such as changes in solar radiation and ambient temperature. In order to improve the efficiency of the PV cell, maximum photovoltaic power tracking (MPPT) is used to adjust the output voltage of the PV system using control techniques that include look-up table, VFM, PFM, POM, and ICM algorithms. The commonly used ICM always regulates the terminal voltages of the PV array according to its value relative to voltage of the maximum power point. The maximum power conditions are [25]

$$\frac{dP}{dV} = 0, \frac{dP}{dI} = 0, \quad \text{and} \quad \frac{dI}{dV} \approx \frac{I - I_o}{(V - V_o)} \tag{4}$$

where $(I - I_{\text{O}})$ and $(V - V_{\text{O}})$ are the incremental changes, I and V are the instantaneous values for the present cycle, I_O and V_O are the stored values at the end of the preceding cycle. MPPT is used to control the input voltage and the duty cycle of the boost converter (dc/dc or dc/ac converter) to ensure maximum power delivery for the PV array. It eliminates any mismatch between the load and the maximum power operating point of the PV array.

In PV energy generation, illumination, temperature, and electrical flows in the PV cell constitute, anomalous diffusion phenomena in inhomogeneous media, and their variation can be expressed as fractional-order electrical production using noninteger derivative-based equations [25]. These anomalous phenomena can be described as fractional-order differentiation. Therefore, (4) can be modified as fractional-order ICM (FOICM). Based on the Grünwald–Letnikov (GL) derivative, we have

$$\frac{d^{\alpha}I(V)}{dV^{\alpha}} = \lim_{\Delta V\to 0}\frac{1}{\Delta V^{\alpha}} \times \sum_{k=0}^{\infty}\frac{(-1)^{k}\Gamma(\alpha+1)}{\Gamma(k+1)\Gamma(\alpha-k+1)}I(V-k\Delta V) \quad (5)$$

where $\alpha > 0$. By considering only the first two terms, we obtain

$$\frac{d^{\alpha}I(V)}{dV^{\alpha}} \approx \lim_{\Delta V\to 0}\frac{I(V)-\alpha I(V-\Delta V)}{\Delta V^{\alpha}}. \quad (6)$$

The incremental changes in current and voltage describe reasonable approximations in fractional-order calculus (FOC). The fractional-order incremental changes of the current and the voltage are approximated as $d\alpha I \approx I - \alpha I_{\mathrm{o}}$ and $dV\alpha \approx \Delta V\alpha = (V - V_{\mathrm{o}})\alpha$, respectively. Therefore, for $0 < \alpha < 1$, the fractional-order incremental conductance is used to express nonlinear dynamic behavior.

For a boost converter and battery charge, the value of duty cycle D that matches the load to the PV array, can be expressed as [25]

$$D = 1 - \frac{(V \pm \Delta V^{\alpha})}{V_L}$$
$$0 < 1 - \frac{V_{\max}}{V_L} < D < 1 - \frac{V_{\min}}{V_L} \quad (7)$$

where V_L is the battery voltage or load voltage, and $V_{\min}$ and $V_{\max}$ are the minimum and maximum values of the input voltage V at the PV array side. The desired voltage is achieved by changing the duty cycle D. At the initial stage, the charging current is maintained at a constant value. After the final voltage of the PV array is reached, the voltage is maintained by slowly decreasing the current. The charging current I_L is stopped when it drops below the threshold value, which is assigned by the manufacturer.

Varying the duty cycle can regulate the input voltage and current. Due to anomalous diffusion phenomena, the incremental changes in voltage or current can be described the reasonable approximations in fractional-order changes.

III. SEDF-Based Voltage Detector

For signal preprocessing applications, chaos synchro-nization (CS) systems are used to detect power quality, voltage disturbances, and control applications, whose behavior can mimic another and appear as different information or abnormal signals [23], [26]–[28]. To achieve synchronization between a master system (MS) and a slave system (SS), the SS asymptotically follows the states of the MS based on the reference information, i.e., the output of the MS. In this study, the Sprott system is considered and its dynamical equation is given by

$$\dddot{x} + a\ddot{x} + b\dot{x} = -1.2x + 2sign(x) + \gamma(t,x) \quad (8)$$

where *sign* (Δ) is the signum function defined by

$$sign(\Delta) = \begin{cases} +1, & \text{if}\Delta \geq 0 \\ -1, & \text{if}\,\Delta < 0 \end{cases} \quad (9)$$

and $\gamma(t,x)$ is a perturbation or uncertain term. The term, γ, is proposed to drive the system state to the desired state, for control purposes. By defining $x_1 = x$, a Sprott-based CS system consisting of a MS and a SS, denoted by the subscripts m and s, can be represented by

$$\begin{cases} \dot{y}_{1m} = y_{2m} \\ \dot{y}_{2m} = y_{3m} \\ \dot{y}_{3m} = -ay_{3m} - by_{2m} - 1.2y_{1m} + 2sign(y_{1m}) \end{cases} \quad (10)$$

$$\begin{cases} \dot{x}_{1s} = x_{2s} \\ \dot{x}_{2s} = x_{3s} \\ \dot{x}_{3s} = -ax_{3s} - bx_{2s} - 1.2x_{1s} + 2sign(x_{1s}) \end{cases}. \quad (11)$$

In tracking the dynamic error states, the terms $\gamma(t,y) = 0$ and $\gamma(t,x) = 0$ are used. The error variables are defined as $e_1 = y_{1\mathrm{m}} - x_{1\mathrm{s}}$, $e_2 = y_{2\mathrm{m}} - x_{2\mathrm{s}}$, and $e_3 = y_{3\mathrm{m}} - x_{3\mathrm{s}}$, and $e = [e_1, e_2, e_3]^{\mathrm{T}}$. Subtracting (11) from (10), the dynamics of the error system can be expressed by

$$\begin{bmatrix} \dot{e}_1 \\ \dot{e}_2 \\ \dot{e}_3 \end{bmatrix} = \begin{bmatrix} 0 & 1 & 0 \\ 0 & 0 & 1 \\ -1.2 & -b & -a \end{bmatrix} e + 2\begin{bmatrix} 0 \\ 0 \\ sign(y_{1m}) - sign(x_{1s}) \end{bmatrix} \quad (12)$$

where $2(sign\,(y_{1\mathrm{m}}) - sign(x_{1\mathrm{s}})) = 0, x_{1\mathrm{s}} = y_{1\mathrm{m}}$ (initial condition), the variables $y_{1\mathrm{m}}$ and $x_{1\mathrm{s}}$ are simultaneous in the positive cycle or the negative cycle for sinusoidal waves. The last two equations form a linear system decoupled from the variable e_1, with the form

$$\begin{bmatrix} \dot{e}_2 \\ \dot{e}_3 \end{bmatrix} = \begin{bmatrix} 0 & 1 \\ -b & -a \end{bmatrix} \begin{bmatrix} e_2 \\ e_3 \end{bmatrix} = [A]\tilde{e}. \quad (13)$$

By having $\mathrm{a} > 0$ and $b > 0$, the robust asymptomatic stability of system (13) is guaranteed.

Referring to (6), a general fractional-order differentiation formulation can be expressed as

$$\frac{d^{\alpha}e(t)}{dt^{\alpha}} = \lim_{\Delta t\to 0}\frac{e(t)-\alpha e(t-t_0)}{(t-(t-t_0))^{\alpha}} \approx \frac{e(t)-\alpha e(t-t_0)}{(\Delta t)^{\alpha}}. \quad (14)$$

The fractional derivative of a function depends on its whole past values. If the parameter α is taken to be 1, then the rate of change is the slope, and for the range 0 to 1, (14) defines the fractional rate of change of the function $e(t)$, as shown in Fig. 3. This shows that the $(t - t_0)$ and t points of a geometric approximation to the αth derivative, and the slope between the curves multiplied by $(\Delta t)\alpha$ is loosely a geometric interpretation of a part of the fractional derivative or fractional rate. In order to describe error dynamics in fractional-order changes, the ordinary

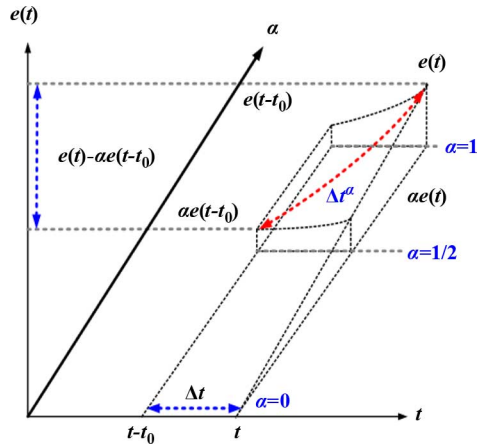

Fig. 3. Geometric interpretation of fractional differentiation for Dt.

differential (11) are modified as fractional-order derivatives, as follows:

$$\begin{bmatrix} D_t^{\alpha} e_2 \\ D_t^{\alpha} e_3 \end{bmatrix} \approx \begin{bmatrix} 0 & t' \\ -b' & -a' \end{bmatrix} \begin{bmatrix} e_2(t) \\ e_3(t) \end{bmatrix} + \begin{bmatrix} 0 & -\alpha t' \\ -\alpha b' & -\alpha a' \end{bmatrix} \begin{bmatrix} e_2(t-t_0) \\ e_3(t-t_0) \end{bmatrix} \quad (15)$$

where the system parameters are modified as

$$t' = \frac{1}{(\Delta t)^{\alpha}}, a' = \frac{a}{(\Delta t)^{\alpha}}, b' = \frac{b}{(\Delta t)^{\alpha}}. \quad (16)$$

The parameter $\alpha = (1-q)$ is the fractional order, satisfying $0 \le q < 1$. When $q = 0(\alpha = 1)$, we have the first-order derivative.

In this study, the fractional-order error equation is used to track various dynamic behaviors of the instantaneous voltage signals at the PV array side. For computer implementation, we define the discrete variables, $y_{2\mathrm{m}} = V_{\mathrm{m}}[i]$ and $y_{3\mathrm{m}} = V_{\mathrm{m}}[i+1]$, $i \in [1, n-1]$, which are based on the data sequence obtained from the desired voltage signal, V_{m}. Similarly, we let the discrete variables, $x_{2\mathrm{s}} = V_{\mathrm{s}}[i]$ and $x_{3\mathrm{s}} = V_{\mathrm{s}}[i+1]$. They are based on the data sequence obtained from the instantaneous voltage signal, V_{s}, stored cycle-by-cycle in the register for online computation. The fraction time (sampling time), $\Delta t = 1/(n \times fs)$, where n is the number of sampling points and $f_{\mathrm{s}} = 1.44$ kHz is the sampling rate. In this study, $n = 24$, where 12 points in positive half-cycle and 12 points in negative half-cycle. So the system (13) can be modified as a discrete error system

$$\begin{bmatrix} \Phi_1[i] \\ \Phi_2[i] \end{bmatrix} \approx \begin{bmatrix} 0 & t' \\ -b' & -a' \end{bmatrix} \begin{bmatrix} e_2[i] \\ e_3[i] \end{bmatrix} + \begin{bmatrix} 0 & -\alpha t' \\ -\alpha b' & -\alpha a' \end{bmatrix} \begin{bmatrix} e_2[i-1] \\ e_3[i-1] \end{bmatrix}, \; i \in [1, n-1] \quad (17)$$

where the error variables are $e_2[i] = V_{\mathrm{m}}[i] - V_{\mathrm{s}}[i]$, $e_3[i] = V_{\mathrm{m}}[i+1] - V_{\mathrm{s}}[i+1]$, $e_2[i-1] = V_{\mathrm{m}}[i-1] - V_{\mathrm{s}}[i-1]$, $e_3[i-1] = V_{\mathrm{m}}[i] - V_{\mathrm{s}}[i]$, and the initial conditions are $V_{\mathrm{m}} = V_{\mathrm{s}} = 0$. The self-synchronization error dynamics formulations (SEDFs) in (17) define Γ_1 and Γ_2 which are used as voltage detectors

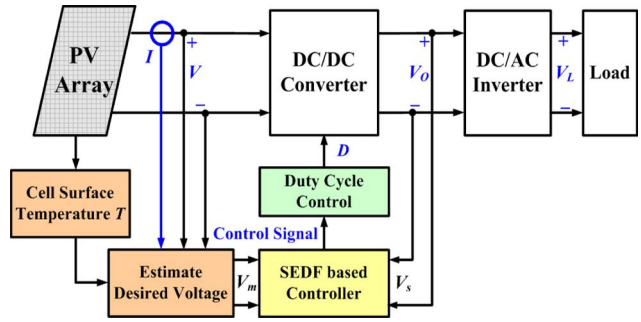

Fig. 4. Block diagram of grid-connected PV conversion system.

for tracking the dynamic errors. They track the fractional-order incremental conductance (FOIC) between the desired voltage, V_{m}, and the instantaneous voltages, V_{s}, cycle-by-cycle. This study uses a converter as a dc transformer, which matches the maximum power by switching the duty cycle, D, using

$$D(p) = D(p-1) \pm \Delta D, \Delta D = \Delta V^{1-\alpha} = \Delta V^{q} \quad (18)$$

where p is the tracking cycle number. Let V_{m} be the desired voltage (constant value), since the instantaneous voltage V_{s} slowly rises, $\Delta V = |V - V_{\mathrm{o}}| = |V_{\mathrm{s}}(p) - V_{\mathrm{s}}(p-1)|$, the motivation of SEDFs (17) is used to track the FOIC in each cycle, which matches the maximum power by switching the duty cycle of the dc/dc converter, adjusting ΔD with (18). When the Γ_1 and Γ_2 achieve the convergent conditions, the control action is terminated.

IV. Implementation of FOSS-Based MPPT Controller

As seen in Fig. 2, the I-V characteristic curves exhibit step variations in the solar radiation and the cell surface temperature. The PV array provides a flexible means of analysis for randomly varying solar radiation and cell surface temperature. At the first stage, the load current or charging current are maintained at a constant value until the MPPV is reached, so, the desired MPPV V_{m} can be estimated for the surface temperature T, and the output current I of PV array, as shown in Fig. 4, and the desired voltage V_{m} can be represented as

$$V = \frac{n_s bTA}{q} \ln\left(\frac{n_p I_{ph} + n_p I_{\mathrm{sat}} - I}{n_p I_{\mathrm{sat}}}\right)] \quad (19)$$

$$V_m = V + \sigma(T_c - 25) \quad (20)$$

where T_{C} is the ambient temperature, and σ is the temperature compensation coefficient. When the dc/ac inverter inputs the load power, P_{L}, into a single-phase grid, the instantaneous power p_{L} is [6], [8]

$$p_L(t) = v_L(t) i_L(t) = \sqrt{2} V_L \sin(\omega t) \sqrt{2} I_L \sin(\omega t) = V_L I_L (1 - \cos 2\omega t) \quad (21)$$

where p_{L} operates at the double angular frequency ω of the grid voltage, V_{L} and I_{L} are the rms values of the grid voltage and current, respectively. Assuming loss-less power transmission from

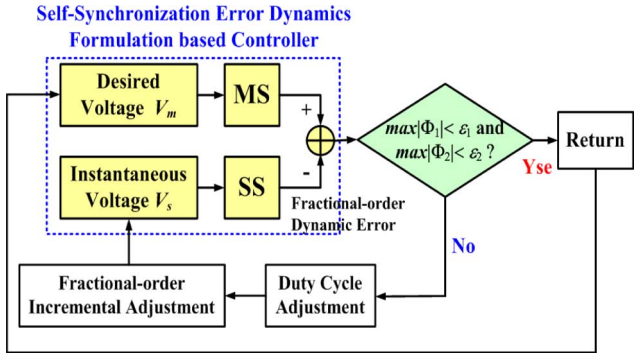

Fig. 5. Block diagram of SEDF-based controller Table I. Specific parameters of the proposed PV array (at solar radiation of 1kW/m2 and a temperature of 25°C) [25].

the solar array to the micro-grid, the power variation is superimposed upon the average of the dc link voltage $V_{\rm o}$. The output current and voltage of the dc/dc converter are expressed as

$$P_{PV(\rm ave)} = P_{\rm grid(ave)} \Rightarrow \frac{V_o}{V_{o(\rm rat)}}\frac{I_o}{I_{o(\rm rat)}} = \frac{V_L}{V_{L(\rm rat)}}\frac{I_L}{I_{L(\rm rat)}}$$
$$\Rightarrow V_{L(pu)} = \frac{V_{o(pu)}I_{o(pu)}}{I_{L(pu)}}, VI = V_oI_o \tag{22}$$

where $V_{\rm o(rat)}$ and $I_{o(\rm rat)}$ are the rated voltage and current of dc/dc converter, $V_{L(\rm rat)}$ and $I_{L(\rm rat)}$ are the rated voltage and current of dc/ac inverter, and overall values are in making per-unit (pu) computations. From (22), $V_{\rm o}(V_{\rm s} = V_{\rm o})$ is the voltage variation due to the output voltage V of the PV array, and the value of V_L also varies with the voltage V_o. The controller updates the voltage $V_{\rm o}$ to match the maximum power (energy conservation: $VI = V_oI_{\rm o}$), so, voltage variation causes the PV current and the boost converter uses the fractional-order incremental adjustment, as shown in Fig. 5. This study uses a boost dc/dc converter as a dc transformer, which matches the optimum load by switching the duty cycle, D, using the (18). When the conditions $\max|\Gamma_1| < \epsilon_1$ and $\max|\Gamma_2| < \epsilon_2$ are met, the controller remains unchanged, where ϵ_1 and ϵ_2 are the tolerance errors, $\epsilon_1 = \epsilon_2 = 10^{-2}$. The Γ_1 and Γ_2 in (17) contain the information of error variables e_2 and e_3, while the system parameters, a' and b', as acceleration coefficients, can quickly guarantee to reach the convergent conditions. The values of the $\max|\Gamma_1|$ and $\max|\Gamma_2|$ will be monotonically decreased and the dynamic errors will reach the specific tolerance error. The controller estimates the desired voltage using the surface temperature and output current measurement. When the atmospheric conditions change significantly, the proposed controller continually performs MPPT.

Solar energy conversion is strongly influenced by solar radiation and the surface temperature of the cell and by the angle of incidence of the sunlight and weather. These phenomena affect the efficiency of solar energy generation. The fractional rates have broad ranges, so by varying the fractional orders, the proposed controller can adapt to uncertain atmospheric conditions.

TABLE I
SPECIFIC PARAMETERS OF THE PROPOSED PV ARRAY (AT SOLAR RADIATION OF 1 KW/M2 AND A TEMPERATURE OF 25 °C) [25]

Specific Parameter	Value
Maximum Power P_{max}	87.7 (W)
Short-circuit Current I_{SC}	4.8 (A)
Open-circuit Voltage V_{OC}	21.7 (V)
Rated Voltage V_R	19.14 (V)
Rated Current I_R	4.58 (A)
Number of Modules Connected in Series n_s	36
Number of Modules Connected in Parallel n_p	1
Short-circuit Current Temperature Coefficient	2.06 (mA/°C)
Open-circuit Voltage Temperature Coefficient	-0.077 (V/°C)

V. EXPERIMENTAL RESULTS AND DISCUSSION

A. Experiment Setup

The proposed controller and traditional methods were designed and tested on a PC Pentium-IV 2.4 GHz with 480 MB RAM and MATLAB software. A small-scale PV conversion system (12 V $\sim$ 24 V) was used for this study, with the relevant specific parameters as shown in Table I, for example, maximum power $P_{\rm max} = 87.7$ W for open-circuit voltage $V_{\rm OC} = 21.7$ V at solar radiation of $1\,{\rm kW/m^2}$ and a temperature of $25\,^\circ$C. However, the solar energy generation is influenced by the solar radiation and cell temperature. The proposed controller can track the maximum power by adjusting the voltage, as the solar radiation and cell temperature increases from $0.2\,{\rm kW/m^2}$ to $1.0\,{\rm kW/m^2}$, and from $25\,^\circ$C to $45\,^\circ$C, respectively. A dc-dc boost converter and a dc-ac inverter were grid connected between the PV array and the local load (110 V/60 Hz) to allow MPPT. The overall control procedure consists of two stages: 1) a MPPT controller maintains operation of the PV array at the maximum power point, 2) a duty cycle control adjust the PV array to deliver maximum power to a micro-grid. The dynamic errors, Γ_1 and Γ_2, are calculated using (17), with the system parameters, a and b, subject to $a > 0$ and $b > 0$, which results in real or complex eigenvalues [23]. When system parameters are selected, the dynamic errors are bounded within limited ranges. By varying the fractional order, q, the proposed controller uses different fractional rates to approach the desired voltage.

For solar radiation of $1\,{\rm kW/m^2}$ and a temperature of $40\,^\circ$C, the maximum power and MPPV are 121.37(W) and 19.86(V), respectively. Fig. 6 shows the desired voltage (0.82 pu) tracking in the time domain and the variation of the dynamic errors with the fractional order $q = 0.2$. The MPPT procedure tracks the maximum point until the convergent condition is reached. For the same atmospheric conditions, the dynamic errors versus the tracking cycles for the fractional orders, $q = 0.1$, 0.15, and 0.3, are shown in Fig. 7(a). It can be seen that the dynamic errors increase slightly as the fractional order increases. Oppositely, the tracking number gradually increases. The average duty cycle is limited from 0.4698 to 0.1807 to control the dc/dc converter, as shown in Fig. 7(b). Figs. 6 and 7 also show stable tracking operations using the fractional orders $q = 0.1 \sim 0.2$. In order to reduce the tracking time and the on/off operations, the fractional order, $q = 0.2(\alpha = 0.8)$, is chosen to implement the fractional-order based controller for MPPT with a trial-and-error method. When the fractional order $q = 0.2$, the FOSS has the system

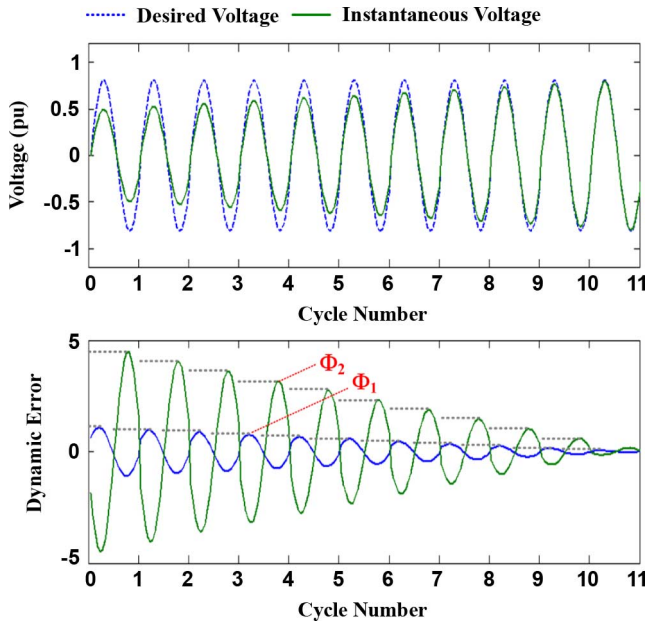

Fig. 6. Desired voltage tracking in the time domain and the variation of dynamic errors F1 and F2 duration of the MPPT (fractional order $q = 0.2$).

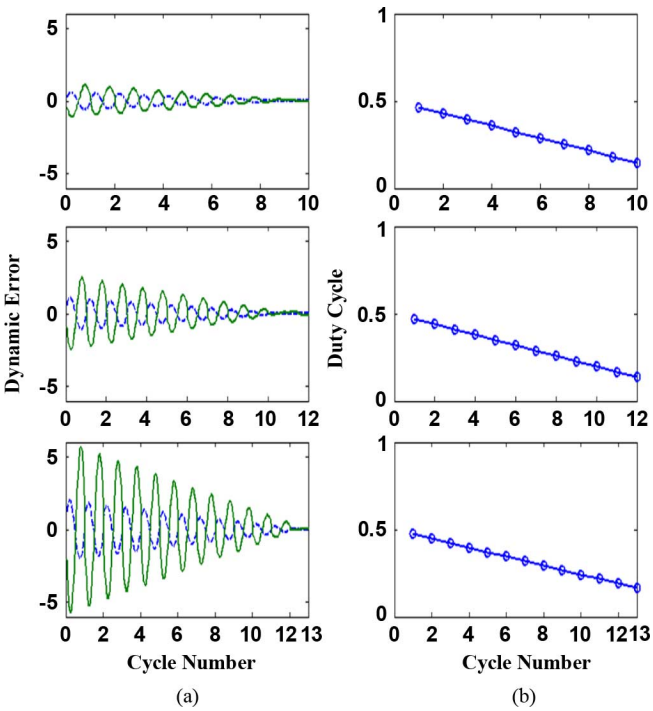

Fig. 7. (a) Dynamic errors versus the tracking cycles with the fractional orders $q = 0.1$, 0.15, and 0.3. (b) Duty cycles versus the tracking cycles with the fractional orders $q = 0.1$, 0.15, and 0.3.

parameters, $a' = 8.5645$ and $b' = 4.2823$, for modeling the voltage detector.

B. Experimental Tests

Fig. 8(a) shows the solar radiation and temperature fluctuating in a stepped distribution. In order to verify the proposed controller, stable and varying atmospheric conditions were used to test the MPPT. As the solar radiation and temperature slowly increase, the FOSS-based controller tracks the maximum

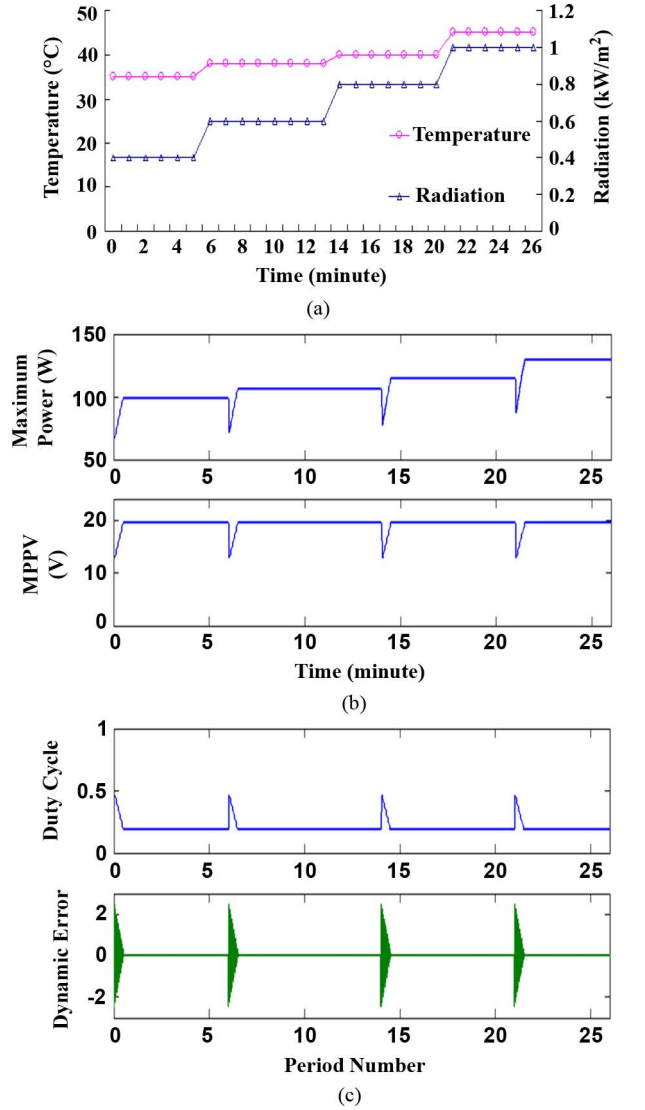

Fig. 8. (a) Solar radiation and temperature with step varying. (b) Experiment results for the PV array power and voltage. (c) Duty cycle versus tracking cycles and dynamic errors versus tracking cycles.

power at each step disturbance. In order to avoid misjudging the working state in the various conditions, the proposed controller launches from the initial voltage/prespecific voltage to MPPV. Each initial value set by sensing the temperature. The initial voltages start from 12 V (half rated voltage) and the proposed controller tracks the maximum power by adjusting the fractional order $(q = 0.2)$ voltage ΔV^q.

For 26 detection periods (52 min), the controller performs MPPT for 2 min of the each sampling period. The solar radiation and temperature increase from $0.4\ \mathrm{kW/m^2}$ to $1\ \mathrm{kW/m^2}$, and from $35\,^\circ\mathrm{C}$ to $45\,^\circ\mathrm{C}$, respectively, so each step variation of the output power tends to the maximum, as shown in Fig. 8(b). It can be seen that the atmospheric conditions obviously change and that the proposed controller has less than 12 tracking cycles in each detection period to perform the MPPT. Fig. 8(c) shows the duty cycle versus the tracking cycles and the dynamic errors versus the tracking cycles. When the atmospheric conditions are stable, the duty cycle of the MPPV also remains unchanged and

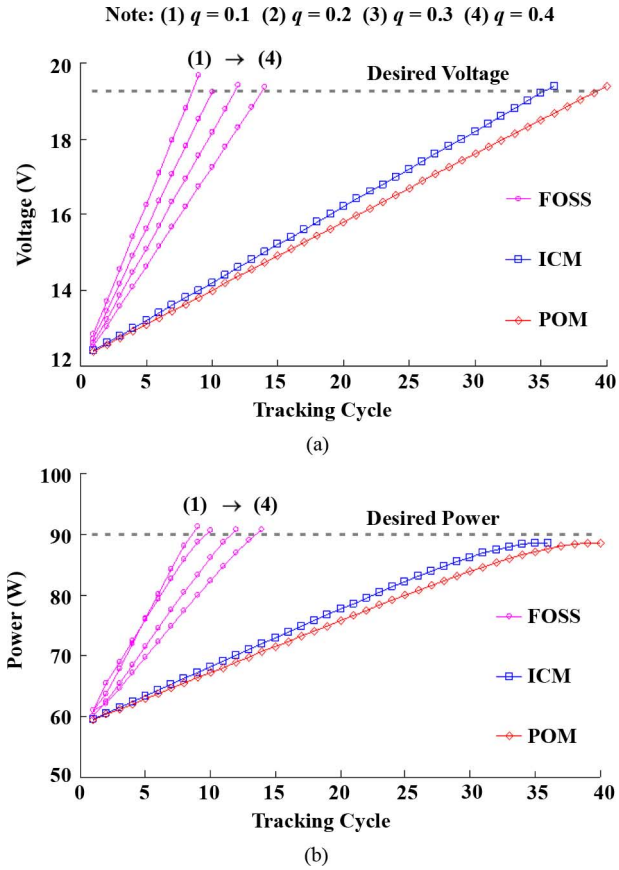

Fig. 9. (a) Desired voltage versus tracking cycle. (b) Desired power versus tracking cycle.

the PV array power delivers steady power to the local load, until the atmospheric conditions change. As observed in the experimental results, the duty cycles have been adjusted until the voltages reach the desired MPPV. The experimental tests confirm that the proposed controller can maintain a maximum power under stable and varying atmospheric conditions.

C. Comparison With Traditional Methods

In a comparison of the proposed method with traditional methods, such as ICM and POM [5], [24], [25], the testing results show that for the same conditions of solar radiation of $1\ \mathrm{kW/m^2}$, and a temperature of $25\,^{\circ}\mathrm{C}$, a voltage at the maximum power point of 19.2 V, an initial voltage of 12 V, the incremental voltages for ICM and POM are $\Delta V = 0.2\ \mathrm{V}$. Fig. 9 shows the experimental results, the voltage versus tracking cycles and the power versus tracking cycles. It can be seen that the proposed method is superior to traditional methods in the number of tracking cycles required (less than 10 cycles) and computing time (average CPU time 16 ms). It uses the $\mathrm{FOIC} = (\Delta V)^{0.2}$ to approach the desired voltage by adjusting the terminal voltage of the dc/dc converter. Each FOIC has large increments, to rapidly track the desired MPPV and to complete the MPPT, as shown in Fig. 9. The tracking number requirement for both ICM and POM depends on the changes in the incremental voltage ΔV. Using a smaller incremental voltage to track the MPPV, they both achieve smaller errors $(< 2\%)$ at the maximum power point, but the tracking number is increased. On the other hand, using a large incremental voltage allows rapid tracking of the maximum power, but it will easily result in perturbation/oscillation around the desired operating point, leading to an unexpected loss.

TABLE II
AVERAGE COMPUTATIONAL ERRORS FOR TRACKING THE MAXIMUM POWER

Atmospheric Condition		Average Error (%)		
Solar Radiation ($\mathrm{kW/m^2}$)	Temperature (^{o}C)	The Proposed Method	ICM	POM
0.2 ~ 0.4	25 ~ 30	1.23	1.03	1.55
0.4 ~ 0.6	30 ~ 35	2.14	1.03	1.52
0.6 ~ 0.8	35 ~ 40	1.62	1.02	1.54
0.8 ~ 1.0	40~ 45	1.17	1.02	2.58

Note: $error(\%) = \dfrac{|P_{\max(act)} - P_{\max(est)}|}{P_{\max(act)}} \times 100\%$, where $P_{\max(act)}$ is the actual maximum power, $P_{\max(est)}$ is the estimated maximum power.

Table II shows the average errors in tracking maximum power. As the solar radiation and temperature increase from $0.2\ \mathrm{kW/m^2}$ to $1.0\ \mathrm{kW/m^2}$, and from $25\,^{\circ}\mathrm{C}$ to $45\,^{\circ}\mathrm{C}$, respectively, the proposed method takes 16 ms $\sim$ 18ms and less than 10 tracking cycles to complete the MPPT, and has a total average error of 1.54%. Though the average errors are slightly greater than those of the traditional methods, the experimental results confirm that the FOSS-based controller can achieve maximum power during solar radiation and temperature changes and can also generate the maximum power at lower solar radiation, including conditions of thin and heavy cloud cover.

In addition, the advantages of using FOSS are 1) easy to obtain self-synchronization error formulation in fractional-order form, 2) easy to determine the system parameters a' and b, resulting in a stable controller, 3) easy to select nonzero system parameters as acceleration coefficients, which control dynamic errors between zero and bounded limit ranges and can guarantee to reach the convergent conditions. However, it is noticed that the power obtained from FOSS (with $q = 0.1 \sim 0.4$) slightly exceeds the desired maximum power. Some further studying will be made and in addition, we will investigate the use of optimization method to determine the optimal parameters, including system parameters and fractional orders. The optimal parameters can enhance tracking accuracy and reduce the tracking time and tracking number.

VI. CONCLUSION

This study proposes a FOSS-based MPPT controller for a small PV conversion system. Under stable and varying atmospheric conditions, the proposed controller reduces the tracking time to less than that required by traditional methods. FOSS is used to track the desired voltage with the convergent condition and can avoid perturbation/oscillation around the desired operating point. Compared with traditional methods, it avoids the use of a regulation algorithm, so it robust in operation, even under conditions of lower solar radiation. The total average error between the estimated and the actual maximum power is less than 2%. The proposed controller reduces the tracking time and the number of tracking cycle required, and is easy to implement

in a programmable microcontroller or an embedded system. The FOSS can also be implemented in nonlinear analog electronic circuits. The efficiency of the PV conversion system is improved for standalone systems or for grid-connected distribution systems, such as battery charging, home power supply, and low-voltage local loads.

REFERENCES

[1] R. H. Lasseter, "Microgrids," in *IEEE Power Eng. Soc.*, Jan. 2002, vol. 1, pp. 305–308.

[2] A. Mellit, M. Benghanem, and S. A. Kalogirou, "An adaptive wavelet-network model for forecasting daily total solar-radiation," *Appl. Energy*, vol. 83, pp. 705–722, 2006.

[3] L. G. Gonzalez, E. Figueres, G. Garcera, and O. Carranza, "Maximum-power-point tracking with reduced mechanical stress applied to wind-energy-conversion systems," *Appl. Energy*, vol. 87, pp. 2304–2312, 2010.

[4] E. Koutroulis and K. Kalaitzakis, "Novel battery charging regulation system for photovoltaic," *IEE Proc. Electr. Power Appl.*, vol. 151, no. 2, pp. 191–197, Mar. 2004.

[5] N. Femia, G. Petrone, G. Spagnuolo, and M. Vitelli, "Optimization of perturb and observe maximum power point tracking method," *IEEE Trans. Power Electron.*, vol. 20, no. 4, pp. 963–973, Jul. 2005.

[6] I.-S. Kim, "Sliding mode controller for the single-phase grid-connected photovoltaic system," *Appl. Energy*, vol. 83, pp. 1101–1115, 2006.

[7] R.-Y. Kim and J.-S. Lai, "A seamless mode transfer maximum power point tracking controller for thermoelectric generator applications," *IEEE Trans. Power Electron.*, vol. 23, no. 5, pp. 2310–2318, Sep. 2008.

[8] J. Eakburanawat and I. Boonyaroonate, "Development of thermoelectric battery-charger with microcontroller-based maximum power point tracking technique," *Appl. Energy*, vol. 83, pp. 687–704, 2006.

[9] J.-M. Kwon, B.-H. Kwon, and K.-H. Nam, "Grid-connected photovoltaic multistring PCS with PV current variation reduction control," *IEEE Trans. Ind. Electron.*, vol. 56, no. 11, pp. 4381–4388, Nov. 2009.

[10] Y.-C. Kuo, T.-J. Liang, and J.-F. Chen, "Novel maximum power point tracking controller for photovoltaic energy conversion system," *IEEE Trans. Ind. Electron.*, vol. 48, no. 3, pp. 594–601, Jun. 2001.

[11] S. Armstrong and W. G. Hurley, "Self-regulating maximum power-point tracking for solar energy systems," in *Proc. 39th Int. Univ. Power Eng. Conf.*, Sep. 6–8, 2004, vol. 1, pp. 604–609.

[12] J.-M. Kwon, K.-H. Nam, and B.-H. Kwon, "Photovoltaic power conditioning system with line connection," *IEEE Trans. Ind. Electron.*, vol. 53, no. 4, p. , Aug. 2006.

[13] A. Pandey, N. Dasgupta, and A. K. Mukkerjee, "High-performance algorithms for drift avoidance and fast tracking in solar MPPT system," *IEEE Trans. Energy Conversion*, vol. 23, no. 2, pp. 681–689, Jun. 2008.

[14] M. Veerachary, T. Senjyu, and K. Uezato, "Feedforward maximum power point tracking of PV systems using fuzzy controller," *IEEE Trans. Aerosp. Electron. Syst.*, vol. 38, no. 3, pp. 969–981, Jul. 2002.

[15] M. Veerachary, T. Senjyu, and K. Uezato, "Neural-network-based maximum-power-point tracking of coupled-inductor interleaved-boost-converter-supplied PV system using fuzzy controller," *IEEE Trans. Ind. Electron.*, vol. 50, no. 4, pp. 749–758, Aug. 2003.

[16] C. A. Otieno, G. N. Nyakoe, and C. W. Wekesa, "A neural fuzzy based maximum power point tracker for a photovoltaic system," in *Proc. 2009 IEEE AFRICON*, Nairobi, Kenya, Sep. 23–25, 2009, pp. 1–6.

[17] C. Hwang, J. F. Leu, and S. Y. Tsay, "A note on time-domain simulation of feedback fractional-order systems," *IEEE Trans. Automat. Control*, vol. 47, pp. 625–631, 2002.

[18] Z. M. Ge and M. Y. Hsu, "Chaos in a generalized Van Der Pol system and in its fractional order system," *Chaos, Solitons, Fractals*, vol. 33, pp. 1711–1745, 2007.

[19] P. Igor, "Fractional differential equations," in *Mathematics in Science and Engineering*. New York: Academic, 1999, vol. 198, ch. 6, 10.

[20] K. S. Killer and B. Ross, *An Introduction to the Fractional Calculus and Fractional Differential Equations*. New York: Wiley, 1993, ch. 6.

[21] J. C. Sprott, "A new class of chaotic circuit," *Phys. Lett.*, vol. 266, no. 1, pp. 19–23, 2000.

[22] D. Almeida, J. Alvarez, and J. G. Barajas, "Robust synchronization of Sprott circuits using sliding mode control," *Chaos, Solitons Fractals*, vol. 30, no. 1, pp. 11–18, 2006.

[23] C.-L. Kuo, "Design of an adaptive fuzzy sliding-mode controller for chaos synchronization," *Int. J. Nonlinear Sci. Numerical Simulat.*, vol. 8, no. 4, pp. 631–636, 2007.

[24] K. H. Hussein, I. Muta, T. Hoshino, and M. Osakada, "Maximum photovoltaic power tracking: An algorithm for rapidly changing atmospheric conditions," *IEE Proc. Generat., Transmiss., Distribut.*, vol. 142, no. 1, pp. 59–64, Jan. 1995.

[25] C.-H. Lin, C.-H. Huang, Y.-C. Du, and J.-L. Chen, "Maximum photovoltaic power tracking for the PV array using the fractional-order incremental conductance method," *Appl. Energy*, vol. 88, no. 12, pp. 4840–4847, Dec. 2011.

[26] H.-T. Yau, C.-L. Kuo, and J.-J. Yan, "Fuzzy sliding mode control for a class of chaos synchronization with uncertainties," *Int. J. Nonlinear Sci. Numerical Simulat.*, vol. 7, no. 3, pp. 333–338, 2006.

[27] C.-H. Huang, C.-H. Lin, and C.-L. Kuo, "Chaos synchronization based detector for power quality disturbances classification in a power system," *IEEE Trans. Power Delivery*, vol. 26, no. 2, pp. 944–953, Apr. 2011.

[28] C.-H. Lin, C.-L. Kuo, S.-J. Chen, J.-L. Chen, and C.-H. Lin, "Chaos synchronization based voltage relays for voltage disturbances detection in a microdistribution system," presented at the Int. Symp. Comput., Consumer, Control, Taichung, Taiwan, Jun. 4–6, 2012.

Chao-Lin Kuo received the B.S. degree from the department of Automatic Control Engineering, Feng Chia University, Taichung, Taiwan, in 1998, and the M.S. degree from the Institute of Biomedical Engineering, National Cheng Kung University, Tainan, Taiwan, in 2000. In 2006, he received the Ph.D. degree in Department of Electrical Engineering, National Cheng Kung University, Tainan, Taiwan.

Currently, he is an Associate Professor of Department of Maritime Information and Technology, National Kaohsiung Marine University, Kaohsiung City, Taiwan, where has been since 2011. His current research interests include intelligent control systems, fuzzy systems, and embedded systems and its applications.

Chia-Hung Lin was born in 1974. He received the B.S. degree in electrical engineering from the Tatung Institute of Technology, Taipei City, Taiwan, in 1998, the M.S. degree in electrical engineering from the National Sun Yat-Sen University, Kaohsiung City, Taiwan, in 2000, and the Ph.D. degree in electrical engineering from National Sun Yat-Sen University, Kaohsiung City, Taiwan, in 2004.

Currently, he is an Associate Professor of Department of Electrical Engineering, Kao-Yuan University, Kaohsiung City, Taiwan, where has been since 2008. His research interests include fault diagnosis in power system, neural network computing and its applications, harmonic analysis, biomedical signal processing, and pattern recognition.

Her-Terng Yau received the B.S. degree from National Chung Hsing University, Taichung, Taiwan, in 1994, and the M.S. and Ph.D. degrees from the National Cheng Kung University, Tainan, Taiwan, in 1996 and 2000, respectively, all in mechanical engineering.

He is currently a Professor in the Department of Electrical Engineering, National Chin-Yi University of Technology, Taichung, Taiwan. His current research interests include energy converter control, system control of mechatronics, nonlinear system analysis and control.

Jian-Liung Chen received the Ph.D. degree in electrical engineering from National Sun Yat-Sen University, Kaohsiung City, Taiwan, in 2003.

Currently, he is an Associate Professor of Department of Electrical Engineering, Kao-Yuan University, Kaohsiung City, Taiwan, where has been since 2010. His research interests include LMI approach in control, robust control, descriptor system theory, digital signal processing, intelligent control systems, and pattern recognition.